RESEARCH ARTICLE

WILEY

Spatially dynamic recurrent information flow across long-range dorsal motor network encodes selective motor goals

Peter E. Yoo[1,3] (ID) | Maureen A. Hagan[9] | Sam E. John[2,3,4] | Nicholas L. Opie[2,3,4] |

Roger J. Ordidge[1] | Terence J. O'Brien[6] | Thomas J. Oxley[3,4,5,6] |

Bradford A. Moffat[1] | Yan T. Wong[7,8,9]

[1]Department of Medicine and Radiology, Melbourne Medical School, The University of Melbourne, Victoria, Australia

[2]Department of Electrical & Electronic Engineering, The University of Melbourne, Victoria, Australia

[3]Vascular Bionics Laboratory, Melbourne Brain Centre, Department of Medicine, The University of Melbourne, Victoria, Australia

[4]The Florey Institute of Neuroscience and Mental Health, Parkville, Victoria, Australia

[5]NeuroEngineering Laboratory, Department of Electrical &Electronic Engineering, The University of Melbourne, Melbourne, Victoria, Australia

[6]Departments of Medicine and Neurology, Melbourne Brain Centre at The Royal Melbourne Hospital, The University of Melbourne, Melbourne, Victoria, Australia

[7]Department of Electrical and Computer Systems Engineering, Monash University, Victoria, Australia

[8]Department of Physiology, Monash University, Clayton, Victoria, Australia

[9]Neuroscience Program, Biomedicine Discovery Institute, Monash University, Clayton, Victoria, Australia

Correspondence
Peter E. Yoo or Bradford Moffat,
Melbourne Brain Centre Imaging Capability,
Department of Medicine and Radiology,
Melbourne Medical School, Kenneth Myer
Building, University of Melbourne, Victoria
3010, Australia.
Email: peter.eli.yoo@gmail.com
or
bmoffat@unimelb.edu.au

Abstract

Performing voluntary movements involves many regions of the brain, but it is unknown how they work together to plan and execute specific movements. We recorded high-resolution ultra-high-field blood-oxygen-level-dependent signal during a cued ankle-dorsiflexion task. The spatiotemporal dynamics and the patterns of task-relevant information flow across the dorsal motor network were investigated. We show that task-relevant information appears and decays earlier in the higher order areas of the dorsal motor network then in the primary motor cortex. Furthermore, the results show that task-relevant information is encoded in general initially, and then selective goals are subsequently encoded in specifics subregions across the network. Importantly, the patterns of recurrent information flow across the network vary across different subregions depending on the goal. Recurrent information flow was observed across all higher order areas of the dorsal motor network in the subregions encoding for the current goal. In contrast, only the top–down information flow from the supplementary motor cortex to the frontoparietal regions, with weakened recurrent information flow between the frontoparietal regions and bottom–up information flow from the frontoparietal regions to the supplementary cortex were observed in the subregions encoding for the opposing goal. We conclude that selective motor goal encoding and execution rely on goal-dependent differences in subregional recurrent information flow patterns across the long-range dorsal motor network areas that exhibit graded functional specialization.

KEYWORDS

7 T, classification, decoding, fMRI, goal encoding, information flow, lower limb, motor planning, motor network

Bradford A. Moffat and Yan T. Wong are the joint last authors.

1 | INTRODUCTION

The dorsal motor network—including the posterior parietal cortex (PPC), the lateral prefrontal cortex (LPFC), the supplementary motor cortex (SMC), and the primary motor cortex (M1)—has been implicated in planning and execution of voluntary movements from human and nonhuman primate studies. Specifically, the PPC and the LPFC (i.e., the frontoparietal regions) have been implicated in movement planning (i.e., motor goal encoding) (Binkofski, et al., 1999; Bremmer, et al., 2001; Connolly, Andersen, & Goodale, 2003; Medendorp, Goltz, Crawford, & Vilis, 2005; Santucci, Kralik, Lebedev, & Nicolelis, 2005; Scherberger, Jarvis, & Andersen, 2005; Siegel, Donner, & Engel, 2012; Siegel, Buschman, & Miller, 2015; Wang, 2008) and movement control (Archambault, Caminiti, & Battaglia-Mayer, 2009; Gaveau, et al., 2014; Glover, Miall, & Rushworth, 2005). On the other hand, the SMC has been implicated in executive-control functions, such as, motor preparation and error monitoring (Cunnington, Windischberger, Deecke, & Moser, 2002; Isoda and Hikosaka, 2007; Nachev, Rees, Parton, Kennard, & Husain, 2005; Picard and Strick, 2001; Ridderinkhof, Ullsperger, Crone, & Nieuwenhuis, 2004; Tanji and Shima, 1994; Ullsperger and von Cramon, 2001).

However, little is known about how the long-range dorsal motor network areas work together to plan and execute specific movements (i.e., selective motor goals) in humans. For example, the predictive activity of the most immanent reach movement observed in the intraparietal sulcus (IPS) neurons of the PPC (Batista and Andersen, 2001) is consistent with the notion that the region is involved in motor goal encoding and movement control. But, IPS neurons have been shown to encode for multiple motor goals in parallel also (Baldauf, Cui, & Andersen, 2008; Medendorp, Goltz, & Vilis, 2006; Wong, Fabiszak, Novikov, Daw, & Pesaran, 2016), suggesting that although the region may contribute to or even be necessary for the cognitive processes, the predictive activity does not imply the sufficiency for or how the activity is linked to the behavior. Similarly, what kinds of information are projected to and how they are utilized by the SMC for performing wide a variety of cognitive functions (Nachev, Kennard, & Husain, 2008) cannot be implied by the isolated epochs of activities during movement preparation and control.

The hypotheses above are dissonant with the traditional view of compartmental functional specialization, which posits that a specific cortical area is largely responsible for a specific cognitive process or behavior (Archambault, et al., 2009; Batista and Andersen, 2001; Gaveau, et al., 2014; Glover, et al., 2005). However, they are in line with recent studies that suggest graded functional specializations of multiple cortical regions subserve the cognitive processes involved in selective voluntary movements (Siegel, et al., 2015; Singer, 2013; Wang, 2008). Thus, investigating how the different areas of the dorsal motor network and streams of cortical information coordinate coherently during movement planning and execution is integral for forming a more holistic model of how we choose to move.

Considering the notion of graded functional specializations with the putatively implicated roles of the dorsal motor network areas, we propose a novel model of motor goal encoding and execution in the
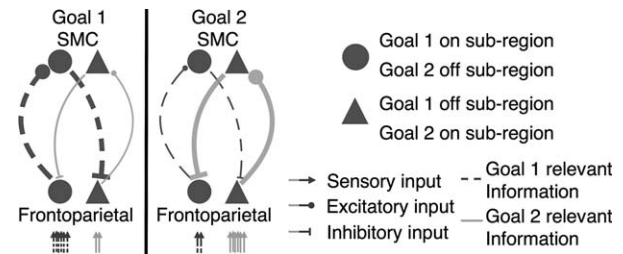
FIGURE 1 Proposed basis of preferential predictive activity during selective motor program planning. Sensory inputs enter into various subregions in the frontoparietal regions at varying levels depending on the current goal. The varying levels of input lead to a cascade of information flow that ultimately facilitate the activity in a given set of subregions while inhibiting that in another through iterative recurrent loops. This process gives rise to predictive on and off subregions or predictive regions for a given goal, and thus leads to encoding of selective motor programs

human dorsal motor network (Figure 1). This model posits that streams of task-relevant information extracted early in the higher order sensory cortices enter the frontoparietal regions (Siegel, et al., 2015), then flow recurrently across the higher order areas of the dorsal motor network (the PPC, the LPFC, and the SMC), allowing for further extraction, integration, and accumulation of task-relevant information (e.g., semantics of cues, proprioceptive information about the effector position). Importantly, the patterns of recurrent information flow in different subregions across the network vary depending on the goal, which allow the SMC to prepare the dorsal motor network for selective movements by iteratively facilitating the activity in a group of subregions (*on subregions*), while inhibiting the activity in another group of subregions (*off subregions*) in a goal-dependent manner. Such spatially dynamic patterns of recurrent information flow give rise to predictive premovement activity in a given group of subregions through a series of positive and negative feedback loops, which in turn, allow for selective motor goals to be encoded across the network. The SMC then feeds the corresponding information forward to the M1 for execution. During the movements, the varying patterns of subregional recurrent information flow continues, allowing the higher order areas to collectively perform movement control by monitoring the accumulating information and modulating the activities in the subregions across the network accordingly.

We provide compelling evidence for the proposed model above by demonstrating the coordination of coherent information flow across the dorsal motor network areas during motor goal encoding and execution for the first time. Using the acquisition parameters that we have optimized for high-spatiotemporal resolution cortical network functional magnetic resonance imaging at 7 T (7T-fMRI) (Yoo, et al., 2017), we recorded blood-oxygenation-level-dependent (BOLD) activity across the dorsal motor network of nine participants during a cued lower limb motor task. We identified the regions involved in movement planning and execution, and the predictive subregions within the dorsal motor network. Then, we compared the spatiotemporal dynamics of information flow across the network and the information about each experimental stage was decoded, after performing hemodynamic

deconvolution to control for the confound of region-specific hemodynamic response functions (HRFs).

We show that both on and off subregions in the PPC, the LPFC, and the SMC all encode task-relevant information initially regardless of the movement type, then a selective motor goal is encoded subsequently only in the on subregions. The spatiotemporal dynamics of recurrent information flow differ across the on and off subregions of the higher order areas depending on the goal. These results together suggest that spatially dynamic recurrent information flow patterns across the long-range dorsal motor network are crucial for selective motor behavior and provide compelling evidence for the proposed model.

2 | MATERIALS AND METHODS

2.1 | Participants

Nine neurologically normal right-footed volunteers (6 males and 3 females; mean ± standard deviation age: 25.4 ± 3.27 years) participated in a single-session fMRI experiment. Each participant gave informed consent prior to their participation. The data was anonymized before the analyses. The University of Melbourne Human Ethics Committee approved this study (Ethics ID: 1340926.1).

2.2 | Image acquisition

All imaging was performed on a 7 T research scanner (Siemens Healthcare, Erlangen, Germany) with a 32-channel head-coil (Nova Medical Inc., Wilmington MA, USA). Whole-brain high-resolution T_1-weighted anatomical images were acquired for each participant using magnetization-prepared rapid gradient echo sequence (Siemens Healthcare prototype research sequence; MP2RAGE (Marques, et al., 2010); voxel volume (VV) = 0.9 × 0.9 × 0.9 mm³; iPAT factor = 4; TR = 4,900 ms; transmitter voltage (TX) = 240 V). High-resolution T_2^*-weighted anatomical images were acquired to calculate susceptibility weighted image (SWI; axial 3D-GRE, echo time (TE)/repetition time (TR)/acquisition time (TA) = 15.3 ms/20 ms/8:42 min, flip angle (FA) = 13°, GRAPPA factor = 3, matrix = 768 × 600 × 120, VV = 0.3 × 0.3 × 1.2 mm³).

All fMRI images were acquired using 2D gradient echo-echo planar imaging (GE-EPI) with multiband and parallel imaging acceleration (Siemens Healthcare prototype research sequence) with the following acquisition parameters: bandwidth = 1980 Hz/pixel; TE = 30 ms; TR = 500 ms; echo spacing = 0.67 ms; EPI factor = 148; phase encoding shift factor = 2; voxel volume = 1.5 × 1.5 × 1.5 mm³; in-plane field of view (FOV) = 224 × 224 mm²; FA = 38°, where T_1 = 2,000 ms; partial Fourier = 6/8; acquisition direction = A-P; multiband factor = 3; GRAPPA factor = 3; number of slices = 21; slice FOV = 31.5 mm. Although minimum TE was 15 ms, 30 ms was chosen based on previous studies where the physiological/thermal noise ratio (Triantafyllou et al., 2005, figure 8b), t value and percent signal change (%SΔ) were shown to peak at ∼30 ms (van der Zwaag et al., 2009, figure 3b,c, respectively) and also to reduce the contribution of BOLD signals arising from distant macrovascular veins (Geißler, et al., 2013; Kennerley, Mayhew, Redgrave, & Berwick, 2010).

### 2.3 | fMRI experiment protocol

The participants engaged a cued ankle-dorsiflexion task. To minimize head movements, participants' legs were slightly raised onto a support foam and strapped at the level of the mid-tibia. Participants followed the instructions on the screen during the motor tasks (Figure 2a), which were also verbally explained prior to scanning. Otherwise they were asked to remain as still as possible. Before the task began, the words "ARE YOU READY?" were presented for 30 s. A trial consisted of a 12 s-rest block with a flashing fixation cross (white to red; 1 Hz), followed by a 3 s prompt block with a visual cue, either "LEFT ANKLE" or "RIGHT ANKLE," indicating which ankle was to be moved. Last, a 5 s execution block was presented where the word "GO" appeared above the persisting prompt cue. The prompt cue flashed at the rate of 1 Hz. The two conditions, left ankle (LA) and right ankle (RA), were repeated four times. The order of conditions was randomized once. All experiments finished with 15 s of rest block. The flashing rate of the prompt cue in the execution blocks served as a guide of movement speed. The flashing of the fixation cross during the rest blocks served to control for the spatial attention and color processing activity evoked by the flashing during the execution blocks.

2.4 | Terminology

For a subregion that exhibits predictive BOLD activity during planning of a given type of ankle movement (Section 2.6.1), the trial blocks of the corresponding ankle movement planning are referred to as the on trials, and the trial blocks of the opposite ankle movement planning are referred to as the off trials (Figure 2b). For example, for the voxels encompassing the subregions showing preferential BOLD activity for left ankle movement planning over right ankle movement planning (i.e., predictive activity for left ankle movement), the LA trial blocks are the on-trials, and the RA trial blocks are the off-trials, and vice versa. By that effect, for a given trial block, the set of subregions exhibiting predictive BOLD activity for the corresponding ankle movement type are referred to as the on subregion, while the set of subregions exhibiting predictive BOLD activity for the opposite ankle movement type are referred to as the off subregion. Ipso facto, the on subregion for a given ankle movement type is the off subregion for the opposite ankle movement type. For example, a set of subregions exhibiting predictive activity for left ankle movement is the left ankle on subregion and also the right ankle off subregion, and vice versa (Figure 2b).

2.5 | fMRI analysis

The FMRIB's Software Library's (FSL v5.0.9) fMRI Expert Analysis Tool (FEAT v6.00) (Jenkinson, Beckmann, Behrens, Woolrich, & Smith, 2012) was used for functional analyses. All functional images were motion corrected, high-pass filtered (0.01 Hz), and optimally skull-stripped, but not smoothed. No slice-timing corrections were employed given the fast TRs and the use of multiband acceleration.
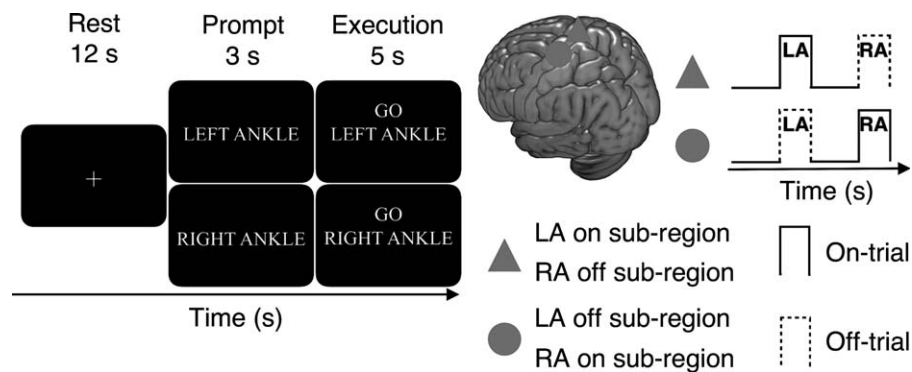
FIGURE 2 Proposed basis of preferential predictive activity, the behavioral task, and the dorsal motor network activation. (a) Cued ankle dorsiflexion task. A fixation cross was presented for 12 s, followed by a 3 s visual prompt indicating which ankle was to be moved, then a 5 s visual prompt to cue the execution of ankle movements. The two conditions—left ankle (LA) and right ankle (RA)—were each repeated four times. (b) Depiction of the terminology used in the current manuscript. For the subregions that activated during left ankle movement planning, the time in which the LA trial-blocks were presented is referred to as the on-trials while the time in which the RA trial-blocks were presented is referred to as the off-trials, and vice versa. Similarly, during the LA on-trials, the subregions that activated preferentially during the left ankle movement planning are referred to as the on subregions while that activated preferentially during the right ankle movement planning are referred to as the off subregions, and vice versa. Thus, LA on subregion is synonymous with RA off subregion and vice versa

To delineate the voxels in regions corresponding to motor goal encoding from motor goal execution, the prompt and execution blocks were modeled separately for the multiple regression analyses. Furthermore, to preserve the close temporal differences between the regressors, the boxcar functions were not convoluted but delayed by 4 s to cater for the hemodynamic response delay (Cunnington, Windischberger, Robinson, & Moser, 2006; Yoo, et al., 2017).

The Z score maps for the prompt blocks were contrasted against baseline (i.e., prompt > rest). The Z score maps of left ankle (LA) and right ankle (RA) execution blocks were contrasted against each other (i.e., LA > RA and RA > LA), to isolate the putative contralateral activation of the M1 during unilateral limb movements and to avoid areas that underlie higher order area cognitions that activated during both conditions from being modelled (e.g., the SMC, the PPC, and the LPFC). Significant activation was defined using a lower Z-score threshold of 2.3 (with $p < .01$ for significance testing; cluster-based correction). These significant activation maps were masked with participant-specific motor region of interest (mROI) masks to ensure fair comparisons of BOLD spatiotemporal dynamics within the dorsal motor network across participants. The mROI masks for the PPC, the LPFC, the SMC, and the M1 were created using FSL and Advanced Normalization Tools (ANTs) (Avants, Tustison, & Song, 2011) in the following steps.

Probability maps of the M1, the SMC, the LPFC, and the PPC in MNI space were each derived from the Harvard-Oxford cortical structural atlas (Desikan, et al., 2006). These maps were thresholded with a lower limit of 25% to reduce the mask spilling into neighboring cortical regions. The resulting images were each binarized to create an mROI mask for each region. MNI_152_1 mm brain image was nonlinearly registered to participant's SWI magnitude image using ANTs. Participants' SWI were linearly registered to their functional images. Using the warp and affine registration information acquired from the above steps, the mROI masks in MNI space were registered nonlinearly to the SWI magnitude space, then linearly to each of the EPI spaces at the individual

level using ANTs. In turn, four mROI masks were created for each participant. The prompt > rest contrast was masked with the PPC, the LPFC, and the SMC mROI masks, and the LA > RA and RA > LA contrasts were each masked with the M1 mROI mask.

A group-level analysis was also performed. First, a study-specific template brain was created using the T_1-weighted anatomical images via ANTs. Second, the contrast of parameter estimates and the variance maps from the individual-level analysis above were linearly registered into each subject's T_1-weighted anatomical space using boundary-based registration. Third, the resulting images were nonlinearly registered into the study-specific template space using ANTs using a mutual information cost function. Using the resulting images, group-level statistical test was carried out in FSL. Significant activation was defined using a lower Z-score threshold of 2.3 (with $p < .05$ for significance testing; cluster-based correction).

Areas showing preferred premovement activity for one side of the ankle movements over the other were identified by modeling the left and right ankle prompt blocks separately, then contrasting them against the baseline and against each other. Then, a group-level analysis was performed on these contrasts. The exact same methods outlined above were used.

2.5.1 | BOLD activation percent signal change calculation and time-course extraction

First, we calculated the %ΔS in the following way. The BOLD time-course from each voxel was extracted from the preprocessed images using the FSL's built-in command, *fslmeants*, at the individual level. The data were normalized by dividing the signal intensity by the temporal mean signal of the voxel at each time point. The normalized time-course data were averaged across the significant voxels within each mROI and trials using the masks created above. The time-courses of voxels that significantly activated during the prompt blocks were extracted from the PPC, the LPFC, and the SMC. The time-courses of
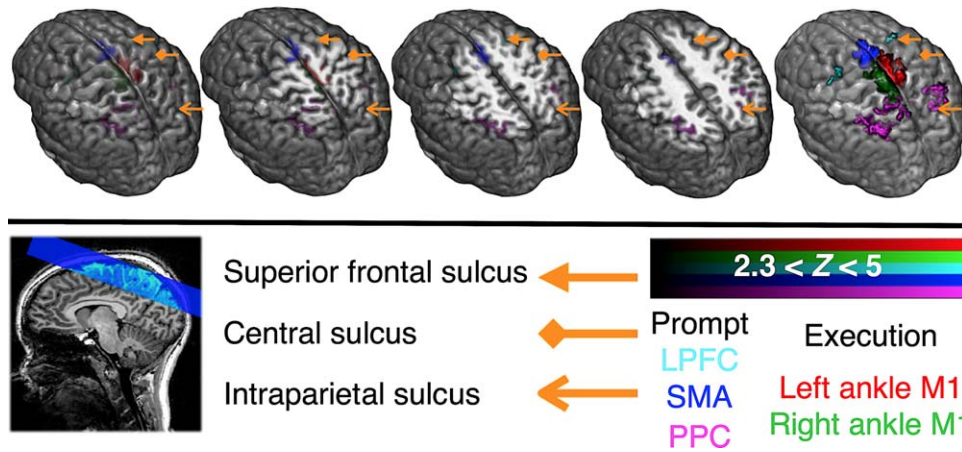
FIGURE 3 Regions of dorsal motor network activation during the cued lower limb motor task Regions of group-level activation overlaid onto the study-specific template brain. Bilateral activation across the LPFC, the SMC, and the PPC was observed during the prompt blocks and highly localized contralateral activation was observed in M1 during the execution blocks at both individual ($Z > 2.3$, $p < .01$; cluster-wise correction) and group-level ($Z > 2.3$, $p < .05$; cluster-wise correction). The first four images from the left show the surface edges of activation at various depths in an oblique direction. The right-most image shows opaque whole clusters of activation for each reign of interest. The sagittal slice functional image in blue overlaid onto the T1-weighted anatomical image in the key panel shows the coverage achieved with all 21 slices. The orange arrows point to the major sulci to aid identification major cortical sites of BOLD activation. The colors of the activation cluster maps denote different areas of activation during prompt or execution blocks. See Supporting Information, Figure 1 for the individual-level activation maps for all participants [Color figure can be viewed at wileyonlinelibrary.com]

voxels that significantly activated during the execution blocks were extracted from the M1.

2.5.2 | Blind deconvolution of voxel-specific hemodynamic response function

We controlled for confound of region-specific HRFs driving the potential differences in spatiotemporal dynamics of BOLD activation across the dorsal motor network. We estimated the HRF of each voxel using a blind approach, then deconvoluted the BOLD signal with the estimated HRF as described in Wu et al., 2013 (Supporting Information, Figure 2). In this method (Wu et al., 2013), the deconvolution is performed as per David, et al. (2008). Assuming that the BOLD signal, $b(t)$, is a convolution of neural states, $s(t)$, with an HRF, $h(t)$:

$$b(t) = s(t) \otimes h(t) + \epsilon(t)$$

where t is the time, $\otimes$ denotes the convolution, and $\epsilon(t)$ is the white noise in the measurement. However, in an absence of simultaneous electrophysiological recordings, the blind-approach substitutes the $s(t)$ with a hypothetical model of neural states $\hat{s}(t)$. A simple on/off model (i.e., delta function) is used to estimate instances of neural events across the BOLD signal time-series by identifying the time-points where the BOLD activity exceeds a threshold in the positive direction. A threshold of 1 standard deviation (SD) above the mean was used in this study. Given the hemodynamic response delay, it is also assumed that the BOLD signal lags behind the peak of neural activation by κ points. κ is defined by searching all integer values from 0 to an arbitrary maximum value (10 s in this instance) and choosing the value that produces the least covariance of noise, $\epsilon(t)$, defined as; $\epsilon = \text{cov}[b(t) - \hat{s}(t) \otimes h(t)]$. This allows to fit $h(t)$ according to $\hat{s}(t)$ simply using a double-gamma function by solving the initial equation above.

Then, approximated neural signal underlying the BOLD activity, $\tilde{s}(t)$, can be calculated using a Wiener filter according to the equation:

$$\tilde{s} = d(t) \otimes b(t)$$

Let $H(\omega)$, $B(\omega)$, $E(\omega)$, and $D(\omega)$ be the Fourier transforms of $h(t)$, $b(t)$, $\epsilon(t)$, and $d(t)$, respectively. Then

$$D(\omega) = \frac{H^*(\omega)}{|H(\omega)|^2 + |E(\omega)|^2}$$

where $*$ denotes the complex conjugate. Then, the true neural states, $s(t)$, can be approximated as $\tilde{s}(t)$ according to

$$\tilde{s}(t) = FT^{-1}\{D(\omega)B(\omega)\} = FT^{-1}\left\{\frac{H^*(\omega)B(\omega)}{|H(\omega)|^2 + |E(\omega)|^2}\right\}$$

where, FT^{-1} is the inverse Fourier transform operator.

2.6 | Statistics

In any cases of multiple comparisons, the significance of the p values was tested against the false-discovery rate (FDR) adjusted threshold using the Benjamini–Hochberg procedure at $Q = 0.05$. For the tests that have survived the FDR-adjusted threshold, the original p values were reported in the text.

2.6.1 | Predictability testing of the preferential premovement activity

We quantified the predictability of the premovement activity from the voxels showing significant preferential activation to selective ankle movements in each region. At the individual level, the %ΔS time-courses were extracted from the voxels showing significant activation during left and right prompt blocks within the PPC, the LPFC, and the

SMC (contrasted against baseline). The data were averaged across voxels, then across left and right ankle trials separately, yielding an average %ΔS time-course during on and off-trials (e.g., on and off-trials for left ankle predicting voxels would be left and right ankle condition trials, respectively, and *vice versa*). The average %ΔS values between 1 s and 7 s after the start of prompt block of on and off-trials were compared across the participants within each region using Wilcoxon rank sum tests. To provide further support, random combinations of 10 on and off-trials were sampled across all participants' voxel averaged data for each region and condition. Then, all the on and off-trial data were compared, without averaging across the trials, within each region and condition using a Wilcoxon rank sum test. This process was permuted 10,000 times with no repeating combinations of trials. The average percentage of significant predictive activity (i.e., on-trials > off-trials) was calculated across permutations for each region and condition.

2.6.2 | Effective connectivity analysis: Multivariate granger causality analysis (MVGC)

We investigated how the patterns of dynamic recurrent information flow changed across the subregions of higher order dorsal motor network areas. We subjected the voxel and trial averaged %ΔS time-courses from the subregions showing nonpredictive and predictive pre-movement activity to a Multivariate Granger Causality (MVGC) analysis with The MVGC Multivariate Granger Causality Matlab® Toolbox (Barnett and Seth, 2014). Data from the nonpredictive subregions were averaged across all 8 trials. Data from the predictive subregions were averaged across the on and off-trials separately across the two conditions (i.e., 4 trials each for left and right ankle condition, thus, total of 8 trials each for on and off-trials). There were 3 variables (PPC, LPFC, and SMC) and 9 observations (one for each subject). The sample rate was set at 2 Hz (i.e., 500 ms) to match the TR used in fMRI acquisition. Maximum model order was set at 10 as lags >5 s were not expected between the regions considering that the delay between prompt and go blocks were only 3 s. Granger's *F* tests were calculated to compare the G-causality between the regions. The actual model order was used for statistical testing, which in this case was 7 volumes (3.5 s). This is consistent with the current experimental design where the prompt blocks were presented 3 s before the execution blocks. Significance was defined at $p < .05$ with FDR multiple comparisons correction ($Q = 0.05$).

2.6.3 | Comparing the spatiotemporal dynamics of BOLD activation

Given the preferential nature of the predictive subregions and the substantial overlap between the predictive and the nonpredictive regions, the data from the significant voxels encompassing the nonpredictive subregions and the M1 were used for this analysis to avoid the potential bias-effects of overlapping voxels. To investigate the spatiotemporal dynamics of activation through the dorsal motor network, we compared the BOLD activation time-courses across the mROIs. The latency to reach 50%, 80%, and 100% peak %ΔS, and latency to decline to 80% and 50% peak %ΔS for each mROI were compared against each other across participants using Wilcoxon rank-sum tests.

To further provide support of varying temporal dynamics across the identified regions, a series of Wilcoxon rank-sum tests were conducted on each time-point of the voxel and trial mean %ΔS from the significant voxels within each mROI. A 1.5 s sliding window was used to compare the %ΔS against baseline (i.e., stationary 6 s window in the rest blocks). Then, the resulting *p* value time-course was inverted by subtracting the value from 1 (i.e., $1 - p$). Finally, the $1 - p$ curve was cross-correlated to the BOLD %ΔS time-course after averaging across voxels and trials. The correlation coefficient (*r*) between the $1 - p$ and BOLD-activation curve and the delay (i.e., latency to reach peak *r*) within each region was compared across the regions.

2.6.4 | Comparing the spatiotemporal dynamics of task-relevant information flow

We quantified whether the observed spatiotemporal dynamics of BOLD activation onset and offset implied direction of information flows between regions of the dorsal motor network by subjecting %ΔS time-courses to a cross-correlation analysis. The voxel and trial averaged %ΔS time-course from each mROI were cross-correlated against each other within a window between 1 s and 11 s from the start of the prompt block. There were 6 contrasts: PPC versus LPFC, PPC versus SMC, PPC versus M1, SMC versus M1, LPFC versus M1, and LPFC versus SMC. Wilcoxon rank-sum tests were carried out to compare the time to reach peak cross-correlation (i.e., delay) across the contrast. The three statistical tests above were performed using the nondeconvoluted data also to provide support that the observed effects were not potentially driven by the deconvolution process.

2.6.5 | Linear classification of spatiotemporal dynamics of BOLD activation

To investigate whether task-relevant information is reflected by the BOLD activity, the deconvoluted BOLD percent signal change (%ΔS) time-course was subjected to a linear classifier commonly used in brain–computer interfaces.

For each contrast, the %ΔS time-courses from all significant voxels within each mROI were subjected to linear classification using linear discriminant analysis *via* custom script written in MATLAB (MathWorks Inc., Natick MA, version R2015b) at the individual level. Data from each voxel was trained and decoded using all time points with a 500 ms-shifting-window, against an average %ΔS value across a stationary 4 s window in the middle of the rest period (i.e., 11–16 s after start of prompt blocks). At each time-point, the classifier was trained with the data points from all but one trial, within the moving window defined as "1" (i.e., active) and the stationary window in rest period as "0" (i.e., baseline). The classifier then decoded whether the data from the remaining trial was either "1" or "0." This was validated by a leave-one-out cross-validation method, whereby each comparison was permuted by the number of trials of a given block, with no repeats. This process was repeated as the window shifted across time and voxels.

We further quantified whether task-relevant information rose at the same time as the BOLD activation. The decoding performance time-course was averaged across significant voxels within each mROI and trials. Then, a series of cross-correlation analyses were carried out

between the voxel and trial-averaged decoding performance and the %ΔS time-course.

3 | RESULTS

3.1 | Regions of the dorsal motor network activate during planned lower limb movements

For all participants, the PPC (mean volume of activation (VV) ± standard error (SE) across participants; 3692 ± 1041 mm³), the LPFC (430 ± 73 mm³), and the SMC (913 ± 119 mm³) activated bilaterally during the prompt blocks at the individual-level (nonpredictive premovement activity; $Z > 2.3$, $p < .01$; multiple regression with cluster-wise correction; Supporting Information, Figure 1). Bilateral activations in the PPC (VV = 2,600 mm³), the LPFC (228 mm³), and the SMC (1,282 mm³) were also observed at the group-level ($Z > 2.3$, $p < .05$; cluster-wise correction; Figure 3). Visual inspection suggested that the activations were observed in the bilateral superior parietal lobule (SPL) and intraparietal sulcus (IPS; especially in the medial bank; mIPS) in the PPC; pre-supplementary motor area (pre-SMA) and supplementary motor area (SMA) in the SMC; and the premotor cortex (PMC) in the LPFC. At both individual and group levels, the dorsomedial M1 activated contralaterally during the execution blocks of each ankle condition (average VV across the M1 at the individual and group levels; 668 ± 73 mm³ (Supporting Information, Figure 1) and 1759 mm³; Figure 3).

3.2 | Selective motor goals are encoded in distinct subregions in distributed cortical regions

Next, we investigated what kinds of task-relevant information flowed across different subregions (e.g., on and off subregions) of the higher order dorsal motor network areas to investigate how selective motor goals are encoded. Areas activating during selective ankle movement planning were identified by modeling the left and right ankle prompt blocks separately for the fMRI analysis. Significant group-level activations were observed only when the left or right ankle prompt blocks were contrasted over the baseline but not against each other, suggesting that any potential predictive activity was preferential, where a given subregion activated during planning of both ankle movements, but activated to a greater extent during planning of a specific ankle movement type. Group-level activations during the left ankle prompt blocks were observed in bilateral pre-SMA, contralateral SMA-proper, contralateral PMC, and bilateral mIPS (Figure 4a). The same pattern of premovement activity was observed during the right ankle prompt blocks, except bilateral activations were observed in the PMC (Figure 4b).

We then quantified the predictability of the premovement activity in each sub-region of the higher order areas. At the individual level, the BOLD %ΔS time courses were extracted from the voxels showing significant activations during left and right prompt blocks separately, within the PPC, the LPFC, and the SMC. Furthermore, to control for the confound of region-specific hemodynamic response functions potentially driving the observed spatiotemporal dynamics of BOLD

activation and information flow, the HRF of each voxel was estimated and then used to deconvolute the signal (Supporting Information, Figure 2) (Wu, et al., 2013).

Averaging across voxels and trials, revealed predictive premovement activities in subregions of the PPC, the LPFC, and the SMC. The %ΔS values during the prompt blocks of the on trials were significantly greater than those of the off trials in the left ankle on subregions (Section 2.4): in the PPC (mean %ΔS ± SE% across participants for on-trials > off-trials; 0.10 ± 0.00% > 0.06 ± 0.01%; $p = .0001$); the LPFC (0.10 ± 0.01% > 0.06 ± 0.01%; $p = .0001$); and the SMC (0.10 ± 0.00% > 0.07 ± 0.01%; $p < .0001$). The same was observed in the right ankle on subregions: in the PPC (0.10 ± 0.00% > 0.05 ± 0.01%); the LPFC (0.10 ± 0.01% > 0.05 ± 0.01%); and the SMC (0.10 ± 0.00% > 0.7 ± 0.01%; all $p < .0001$; Figure 4c). To further validate the predictability of the preferential premovement activity, we compared the %ΔS of randomly sampled on and off trials across all participants. On average, predictive activity for the left and right ankle movements were observed 94.7 ± 0.2% (mean ± SE%) and 97.5 ± 0.2% of the time in the PPC; 73.8 ± 0.4% and 88.0 ± 0.3% of the time in the LPFC; and 91.3 ± 0.3% and 87.2 ± 0.3% of the time in the SMC, respectively (Wilcoxon rank sum tests; all $p \leq .0443$). These results, along with the nonpredictive premovement activity identified in the earlier section, show that task-relevant information is initially encoded in parallel across different subregions of the higher order dorsal motor network areas, then selective motor goals are subsequently encoded in the on subregions (Figure 4c).

3.3 | Goal-dependent differences in the pattern of recurrent information flow across the dorsal motor network allow for selective motor goal encoding

To investigate how selective motor goals are encoded, we quantified the patterns of directional information flow across the subregions of the higher order dorsal motor network areas. The %ΔS time-courses from the subregions were subjected to an effective connectivity analysis. We took a Multivariate Granger Causality approach (Barnett and Seth, 2014) to test whether the past BOLD activity in a given region, X, contained information that could help predict the future BOLD activity another region, Y (i.e., activity in the X Granger-causes Y), while controlling for multiple comparisons (FDR-adjusted). Thus, G-causal relationships allowed for quantifying the direction of information flow.

Averaging across the significant voxels and trials, recurrent G-causal relationships were revealed between the PPC and the LPFC (i.e., frontoparietal regions), and between the SMC and the frontoparietal regions in the subregions showing nonpredictive premovement activity (all $p \leq .0017$; Figure 5a). In the subregions showing predictive premovement activity (i.e., on subregions), the same pattern of G-causal relationships was observed in the on subregions; however, the recurrent G-causal relationship between the frontoparietal regions was weaker, while that between the frontoparietal regions and the SMC remained strong (all $p \leq .0058$; Figure 5b). Critically, in the off subregions, the bottom–up G-causal relationships to the SMC became weaker, while the top–down G-causal relationships from the SMC to
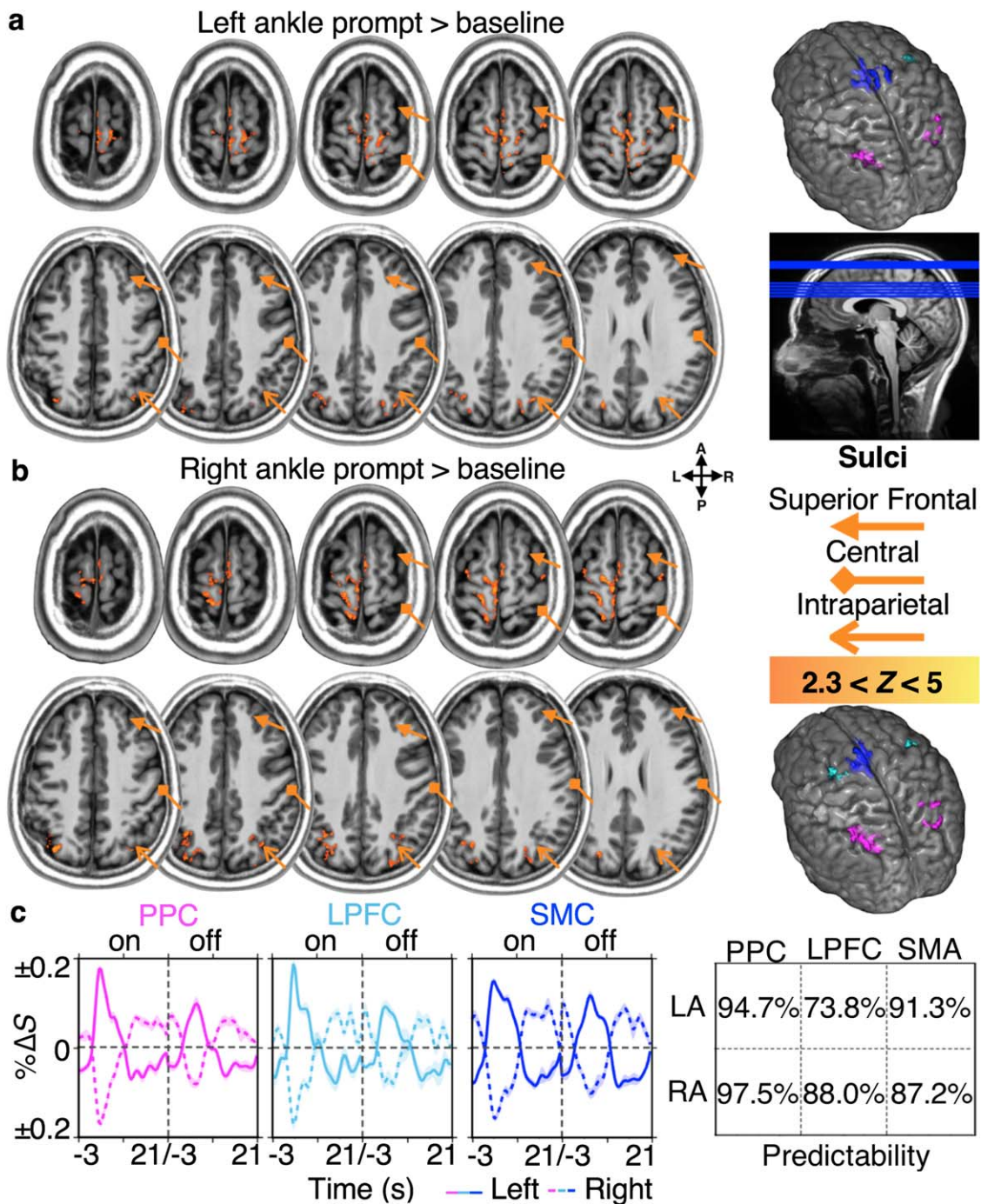
FIGURE 4 Predictive activity in the subregions of higher order dorsal motor network areas. Premovement activity predicting the side of ankle movements was observed in subregions of the PPC, LPFC, and SMC at the group level. Modeling the left and right ankle prompt blocks separately revealed similar, yet different pattern of BOLD activation in the PPC, LPFC, and SMC. (a) Significant activations during the left ankle prompt blocks were observed in the bilateral pre-SMC, contralateral SMC proper, contralateral PMC, and bilateral mIPS. (b) The same pattern of activation was observed for right ankle prompt blocks except there was a bilateral PMC activation. (c) The plots on the left show the participant, voxel, and trial averaged region-specific %ΔS time-courses from the voxels showing predictive activity for left (solid lines) and right (dashed lines) ankle movements, during prompt blocks of on and off trials (left and right column, respectively). The plot on the right shows the average predictability of the premovement activity in each region (all $p \leq .0443$; FDR adjusted). All shading depicts standard error across participants [Color figure can be viewed at wileyonlinelibrary.com]

the frontoparietal regions remained strong, and that between the frontoparietal regions was no longer observed (all $p \leq .0400$; Figure 5c). The exact Granger's F test values and the corresponding p values can be found in Table 1.

These results show that the patterns of recurrent information flow differed across the subregions depending on the current goal. Taken together with the result that the predictive activities were observed across all higher order areas and that they were preferential and not
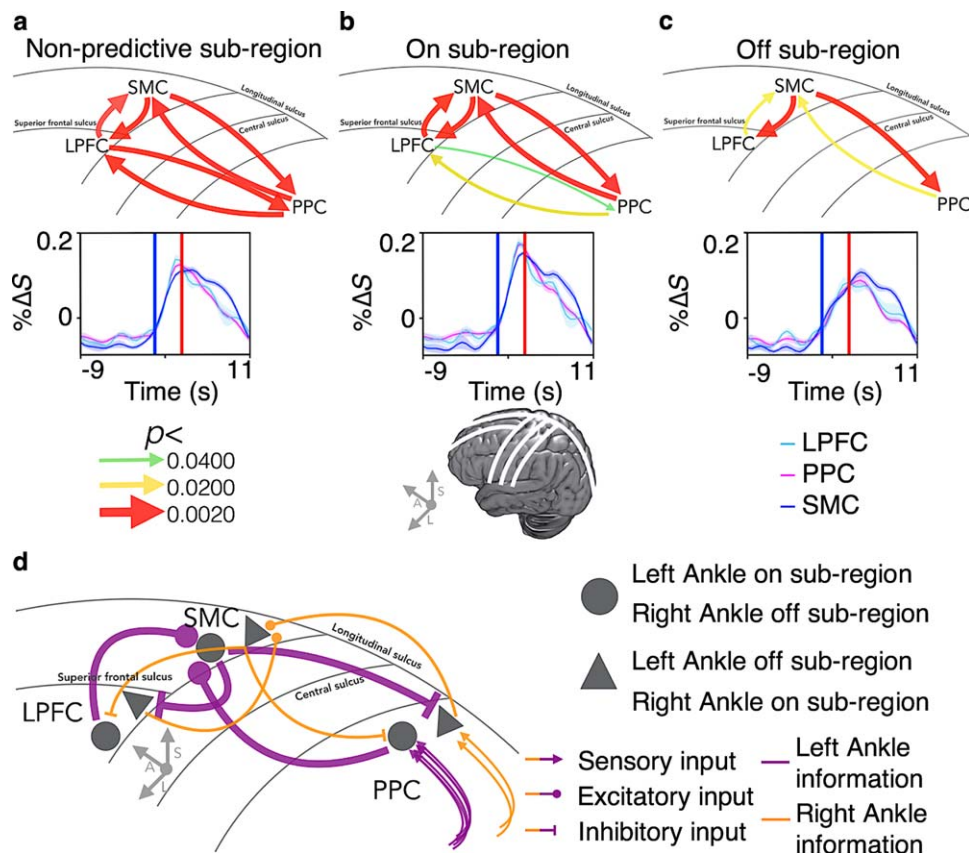
FIGURE 5 Spatially dynamic goal-dependent patterns of recurrent information flow across the dorsal motor network subregions. The pattern of recurrent information flow differed across on and off subregions depending on the current goal. Averaging across the significant voxels and trials, (a) recurrent G-causal relationships were revealed between the PPC and the LPFC, and the SMC and these frontoparietal regions in the subregions showing nonpredictive premovement activity (all $p \leq .0017$). (b) In the subregions showing predictive premovement activity, the same pattern of G-causal relationships was observed in the on subregions; however, the recurrent G-causal relationship between the frontoparietal regions was weaker, while that between the frontoparietal regions and the SMC was the same (all $p \leq .0058$). (c) Critically, in the off subregions, the bottom–up G-causal relationships to the SMC became weaker compared to the on subregions, while the top–down G-causal relationships from the SMC to the frontoparietal regions remained strong, and the recurrent G-causal relationships between the frontoparietal regions was no longer observed (all $p \leq .0400$). The curves below, plot the voxel, trial and participant averaged %ΔS of each region. The up-right blue and red bars denote the start of prompt and execution blocks, respectively. The schematic brains and the lines correspond to the major sulci of the brain labeled on the schematic of the Granger-causality directions. (d) A schematic of potential mechanisms underlying goal-dependent subregional recurrent information flow pattern differences in the predictive regions only, according to the proposed model, an example of right ankle movements [Color figure can be viewed at wileyonlinelibrary.com]

selective, the observed patterns are consistent with our model that suggests the subregional differences in information flow patterns may provide the basis for encoding of specific motor goal via positive and negative feedback loops between the higher order regions (Figures 1a and 3d; see Section 2.2).

3.4 | Task-relevant information appears and decays earlier in the higher order areas than in the M1 during encoding and execution selective motor goals

We then investigated when the task-relevant information appeared and decayed throughout the dorsal motor network by comparing the timing of the BOLD activation onset and offset. Task-relevant information appeared and decayed significantly earlier in the higher order areas than in the M1. Averaging across significant voxels and trials revealed significantly shorter latency to peak %ΔS from the start of the prompt

block in the PPC and the LPFC (average latency $\pm$ standard error (SE); 3.7 ± 0.2 s and 3.8 ± 0.5 s) compared to the SMC (4.9 ± 0.4s; Wilcoxon rank-sum test p values against the PPC and the LPFC, respectively; $p = .0274$ and 0.0291) and the M1 (7.3 ± 0.4 s; $p < .00001$ and $p = .0007$). Further, the latency to peak %ΔS was significantly longer in the M1 than the SMC ($p = .0026$). Consistently, the latency to reach 50% and 80% of peak %ΔS were also longer in the M1 (4.2 ± 0.1s and 5.5 ± 0.3s; all $p < .0001$) compared to the PPC (2.0 ± 0.1 s and 2.6 ± 0.1 s), the LPFC (2.2 ± 0.1 s and 2.8 ± 0.2 s, and the SMC (2.4 ± 0.2 s and 2.9 ± 0.2 s; Figure 6a).

Latency to decline 80% and 50% of peak %ΔS from the start of prompt block was significantly longer in the SMC (7.2 ± 0.4 s and 8.0 ± 0.4 s) than in the PPC (5.1 ± 0.2 s and 6.3 ± 0.3 s; $p = .0004$ and $p = .0042$). Latency to decline 80% of peak %ΔS was also significantly longer in the SMC than in the PPC (5.1 ± 0.6 s; $p = .0145$). The same effect was trending at 50% of peak %ΔS (LPFC: 6.4 ± 0.6;

TABLE 1 *F* and *p* values for Granger's *F* tests conducted during MVGC analysis

	PPC	LPFC	SMC
Non-predictive (*F* value, *p* value)			
PPC		0.10, .0003***	0.10, .0002***
LPFC	0.09, .0008***		0.08, .0017***
SMC	0.16, <.0001***	0.14, <.0001***	
On subregion (*F* value, *p* value)			
PPC		0.07, .0058**	0.11, .0001***
LPFC	0.05, .0400*		0.08, .0011***
SMC	0.12, <.0001***	0.14, <.0001***	
Off subregion (*F* value, *p* value)			
PPC		0.05, .0574	0.06, .0255**
LPFC	0.03, .3296		0.06, .0267**
SMC	0.18, <.0001***	0.10, .0003***	

The values represent G-causal relationships from regions in the rows to columns.
*<0.0400; **<0.0200; ***<0.0020.

$p = .0515$); however, when replacing an outlier (participant 3) of 10 s from the LPFC latency values (6 *SD* away from mean) with the mean, revealed a significantly longer latency in the SMC than the LPFC ($p = .0065$). The BOLD activity also sustained longer in the M1 compared to all other regions (10 ± 0.2 s and 8.7 ± 0.4 s; all $p \leq .0202$). These results further suggest that task-relevant information may rise and decay slightly earlier in the frontoparietal regions than in the SMC (Figure 6c,d).

To further demonstrate the spatiotemporal dynamic differences of BOLD activation across regions, Wilcoxon rank-sum tests were conducted at each time-point with a 1.5 s sliding-window against a stationary 6 s window in the rest blocks. The p values of Wilcoxon rank-sum tests should decrease while %ΔS increases during the experimental blocks as the %ΔS values move further away from the rest block %ΔS value. Then, the time-course of inverse p values (i.e., $1 - p$) should cross-correlate with that of %ΔS without delay. Consistently, averaging across significant voxels and trials revealed significant cross-correlations between the time-courses of the inverse p values and %ΔS in each region with no significant delay (Figure 6b; all $R \geq 0.7 \pm 0.0$, $p \leq 0.0208$; all r peaked within 1 *SD* from 0).

3.5 | Task-relevant information feeds forward from the higher order areas to the M1

We further investigated whether the observed pattern of activity onset and offset implied spatiotemporal dynamics of information flow through the dorsal motor network. The %ΔS time-courses from the significant voxels were subjected to a cross-correlation analysis, which allowed us to measure the delays in correlated activity flowing from one area to the next.

The results show that the task-relevant information feeds forward from the higher order areas to the M1. Averaging across voxels and trials, revealed strong cross-correlations of the BOLD activation time-courses between all regions (participant mean cross-correlation (R) $\pm$ *SE*; all $R \geq 0.9 \pm 0.01$, all $p \leq .0023$; Figure 7a,b). Significant

delays (time-point of peak R) were observed between the M1 and the PPC ($p = .0001$), the LPFC ($p = .0048$), and the SMC ($p = .0003$). Importantly, the delays from the PPC and the LPFC to the M1 (average delay $\pm$ *SE*; 2.6 ± 0.3 s and 2.2 ± 0.3 s, respectively) were significantly longer than the delays to the SMC (0.3 ± 0.1 s and 0.4 ± 0.2 s, Wilcoxon rank-sum test $p = .00001$ and $p = .0004$). The delays from the SMC to the M1 (1.5 ± 0.2 s) were also significantly longer than the delays from the PPC ($p = .0005$) and the LPFC to the SMC ($p = .0040$). Last, the delays from the PPC to the M1 were significantly longer than the delays from the SMC to the M1 ($p = .0053$; Figure 7c). These results further suggest that the task-relevant information may flow sequentially from the frontoparietal regions to the SMC, consistent with the spatiotemporal dynamics of task-relevant information appearance shown in the previous section

3.6 | Task-relevant information is embedded in BOLD signal time-course

Last, to demonstrate that the spatiotemporal dynamics of BOLD activation infers spatiotemporal dynamics of information flow, we investigated whether task-relevant information was embedded in the BOLD signal. The information about the stages of the experiment was decoded from the BOLD signal within each region, by subjecting the significant voxels' %ΔS time-courses to a linear classifier. At each time-point, the classifier was trained using the data from all but one trial and the data from the remaining trial was decoded against a stationary 4 s window in the middle of rest block (i.e., average %ΔS between 14 s and 18 s after the start of prompt blocks). For each comparison, leave-one-out cross-validation method was used with no repeats.

Maximum decoding performance of each trial, averaged across trials, and participants were 97% $\pm$ 1%, 97% $\pm$ 1%, 91% $\pm$ 3%, 78% $\pm$ 3%, and 93% $\pm$ 2% for the right M1 (corresponding to LA), left M1 (corresponding to RA), the PPC, the LPFC, and the SMC, respectively (Figure 8a, bottom row). Furthermore, averaging across voxels and trials revealed significant cross-correlations between the time-courses of decoding performance and %ΔS with no delay within each region (Figure 8b; Correlation coefficient (R) $\pm$ SE; 0.9 ± 0.01 ($p = .0009$), 0.9 ± 0.02 ($p = .0009$), 0.8 ± 0.02 ($p = .0096$), 0.7 ± 0.04 ($p = .0358$), and 0.9 ± 0.02 ($p = .0009$); all R peaked within 2 *SD* from 0). These results show that task-relevant information can be inferred from HRF-controlled BOLD signal, and importantly, that it appears and decays with the same spatiotemporal dynamics as the %ΔS time-course.

4 | DISCUSSION

We systematically show how the human dorsal motor network areas coherently encode and execute selective motor programs for the first time. The results provide compelling evidence for our proposed model, which hypothesizes that selective motor goal encoding and execution rely on goal-dependent subregional differences in recurrent information flow patterns across the long-range dorsal motor network areas exhibiting graded functional specializations. The voxel-wise HRF deconvolution and consistent results across numerous measures of
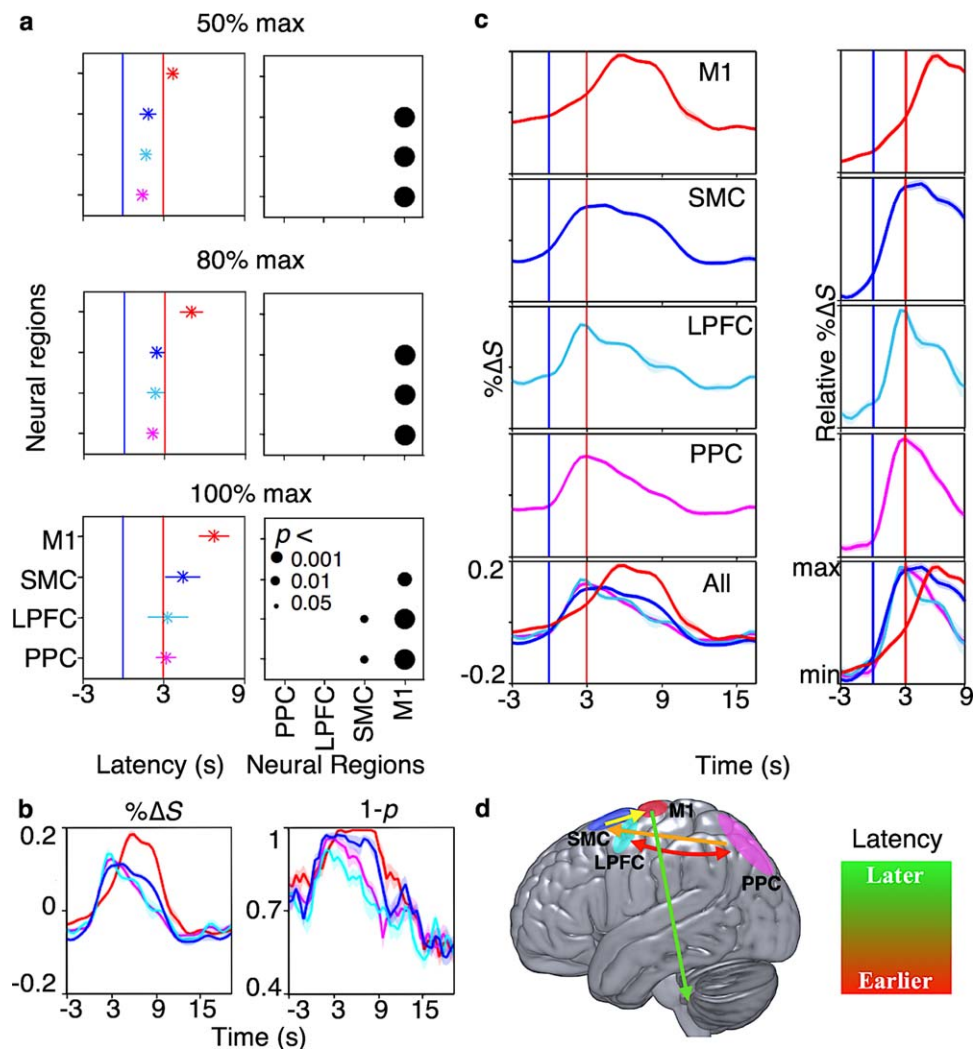
FIGURE 6 Sequential appearance of task-relevant information from the higher order regions of the dorsal motor network to the M1. Movement information rose and decayed earlier in the higher order regions of the dorsal motor network than in the M1. It decayed in the frontoparietal regions soon after it appeared in the SMC while it persisted throughout movements in the SMC. The frontoparietal regions had the shortest latency values followed by SMC then M1 (all $p \leq .0291$). (a) Left figures show the average latency to reach 50% (top), 80% (middle), and 100% (bottom) maximum %ΔS from the start of the prompt block across the cortical regions. Right figures show the p values of Wilcoxon rank-sum tests comparing the latency values across participants. (b) The participant, voxel, and trial average of %ΔS time-course (left) and time-course of inverse p values (i.e., $1 - p$) of Wilcoxon rank-sum tests at each time point with a sliding 1.5 s window against a stationary 6 s window in rest blocks (right). Significant cross-correlations with no delay were observed between %ΔS and $1 - p$ within each region (all $R \geq 0.7$, $p \leq .0358$; all R peaked within 1 SD from 0). (c) Left plots show average time-course of %ΔS from significant voxels. Each row represents one cortical region. The last row shows the time-courses of all regions. Right plots show the average %ΔS normalized to its relative minimum and maximum values to highlight the temporal dynamic differences across the regions. (d) A schematic representation of potential flow movement plan and execution, as represented by the latencies. The blue and red bars in (a) and (c) indicate the start and duration of prompt and execution blocks, respectively. The shading in (a) and (b) depict standard errors and error bars in (c) depict standard deviations across participants [Color figure can be viewed at wileyonlinelibrary.com]

spatiotemporal dynamics of information flow provide further support for the proposed model.

As our model posits, the results show that the task-relevant information begin to accumulate across diffuse subregions of dorsal motor network areas, as evident from the initial rise in BOLD activity in both on and off subregions in the PPC, the LPFC, and the SMC. Then, a given motor goal is subsequently encoded in a specific set of subregions across the network yielding predictive premovement activity, where the activity continued to increase only in the on subregions

of the current goal while that in the off subregions declined. The initial information accumulating in both the on and off subregions may reflect encoding of shared information between the two goals. High degree of similarity between the two motor goals and the visual stimuli presented in each condition is consistent with the notion above.

Importantly, our results show for the first time that the pattern of recurrent information flow across the network varies across the subregions in a goal-dependent manner, which may explain how the on and off subregions emerge, and thus, how selective motor goals are encoded.
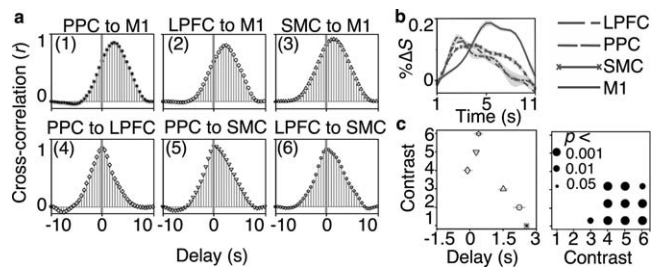
FIGURE 7 Cross-correlation of BOLD activation time-courses across various regions after blind-HRF deconvolution. Task-relevant information flowed sequentially from the higher order regions to the M1. Averaging across significant voxels and trials revealed significant cross-correlations of %ΔS time-courses across all regions (all $R \geq 0.9 \pm 0.0$, all $p \leq .0023$). Wilcoxon rank-sum tests revealed significant cross-correlation delays between regions from the PPC and the LPFC to the M1, and the SMC to the M1 (all $p \leq .0048$; FDR corrected at $Q = 0.05$). Of note, the delays from the PPC and the LPFC to the M1 were significantly longer than the delays to the SMC (all $p \leq .0004$). The delays from the SMC to the M1 were significantly longer than the delays from the PPC and the LPFC to the SMC ($p \leq .0040$). Furthermore, the delays from the SMC to the M1 were significantly longer than the delays from the PPC to the M1 ($p = .0053$). (a) Each box shows the participant average cross-correlations between the voxel and trial averaged %ΔS time-courses in various cortical regions (i.e., contrasts) with different delay periods. (b) The average %ΔS time-course within the window of time that was used for cross-correlation calculations (nonmasked window). (c) The left figure shows the participant average delay to reach maximum cross-correlation coefficient for each contrast. The error bars depict standard errors in delays across participants. The markers correspond to the contrasts shown in (a). The right figure shows the p values of pairwise Wilcoxon rank-sum tests comparing delay values between the contrasts across participants, after FDR correction at $Q = 0.05$

The recurrent information flow in the on sub-regions sustained across all higher order areas of the dorsal motor network during the on-trials (Figure 5b). On the other hand, in the off subregions, the bottom–up information flow to the SMC became weaker while the top–down information flow from the SMC to the frontoparietal regions remained strong, and the recurrent information flow between the frontoparietal regions were no longer observed (Figure 5c). These results suggest that the SMC monitors the accumulating information and modulates the activity across the higher order areas to encode selective motor goals, where it facilitates the activity in the on subregions and inhibits the activity in the off subregions according to the current goal in an iterative manner. The spatiotemporal dynamics of the task-relevant information rising and decaying slightly earlier in the frontoparietal regions compared to the SMC are consistent with the notions above. Furthermore, early frontoparietal activation during movement planning has been previously reported in a non-human-primate study that simultaneously measured spiking activity across the cortical motor network regions (Siegel, et al., 2015).

Considering the notions above, along with the current experimental design, provides further insights into how the higher order areas of the dorsal motor network may also collectively, but not individually, engage in movement control using the same principles as above. The

current task demanded a constant perception of visual cues to initiate, perform, and terminate selective ankle dorsiflexions. Furthermore, the same prompt cue was presented in both the prompt and execution blocks (Figure 2a). If indeed the subregions of the frontoparietal regions specialize in movement monitoring and control (Archambault, et al., 2009; Gaveau, et al., 2014; Glover, et al., 2005), then the activity in these regions should have persisted throughout the movements. Instead, the activity in the frontoparietal regions subsided, while it sustained in the SMC throughout the movements, highlighting the graded nature of the regions' functional specializations during voluntary movements.

These results suggest that a series of feedback loops between the on and off subregions of the higher order areas iteratively allow the SMC to modulate the activity across the network to encode and control selective motor goals according to the accumulating information in the frontoparietal regions. Specifically, we propose that at the macroscopic level, there are positive feedback loops between the on subregions across the higher order areas and negative feedback loops between the on and off subregions, and that the level of inputs from the higher order sensory cortices to each subregion vary depending on the goal. For example, relatively more task-relevant information specific to the current goal are extracted compared to the information that are specific to, or shared with another goal, in turn, the level of input to the on subregions becomes greater than the off subregions over time. Then, the positive feedback loop allows the activity to build-up in the
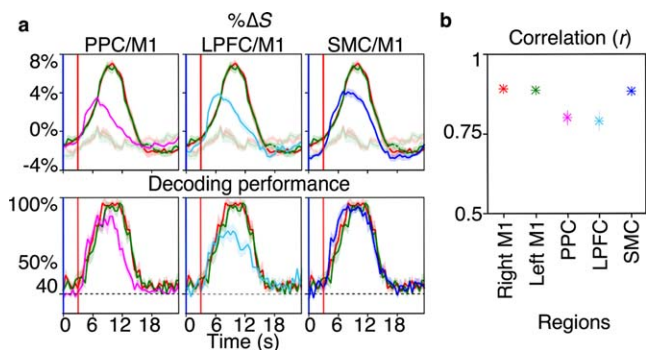
FIGURE 8 Decoding performance of fMRI-based linear classification after blind-HRF-deconvolution. Task-relevant information could be inferred from the BOLD activity, and importantly, it appeared and decayed with the same spatiotemporal dynamics as per BOLD activation. Averaging across significant voxels and trials, decoding performance increased with BOLD activity within each region, where strong cross-correlations were observed between the time-courses of decoding performance and %ΔS with no delay (all $R \geq 0.7$, $p \leq .0358$; all R peaked within 2 SD from 0). (a) Voxel, trial, and participant average %ΔS (top row) and decoding performance (bottom row) time-course in the PPC, the LPFC, and the SMC (left to right) overlaid on top of that of the M1. The faded curves plot the average %ΔS time-courses during the opposing trials in the same M1. The shading indicates the standard error across participants for each corresponding measure. The blue and red up-right lines represent the start of prompt and execution blocks, respectively. (b) Participant average peak cross-correlation values between %ΔS and decoding performance time-courses. Error bars indicate standard errors across participants [Color figure can be viewed at wileyonlinelibrary.com]

on subregions, while the negative feedback loop centered around the SMC iteratively inhibits the activity in the off subregions (Figures 1 and 5d). The initial rise in off subregion activity followed by the subsequent decay supports the notions above.

Consistently, previous studies have shown that task-relevant information is first extracted in the higher order sensory cortices before they are projected forward (Siegel, et al., 2015), providing the basis for varying levels of subregional inputs that depend on the goal. The SMC, especially the pre-SMA, has been repeatedly shown to be involved in tasks that require executive-control functions in humans (Picard and Strick, 1996, 2001). Robust activation in the human pre-SMA is often observed during tasks that require inhibition of task-irrelevant and/or conflicting information (i.e., Eriksen flanker task and Stroop-task) (Nachev, et al., 2005; Ridderinkhof, et al., 2004; Ullsperger and von Cramon, 2001). Lesion studies further provide compelling evidence of the human SMC's involvement in the executive-control function role, where a localized SMC damage has partly or specifically led to negative motor dysfunctions, such as motor neglect and gait apraxia (Della Sala, Francescani, & Spinnler, 2002; Krainik, et al., 2001). Previous non-human-primate studies also show consistent results, where excitatory microstimulation of the pre-SMA reduced erroneous responses when they had to inhibit the current motor goal to switch the saccade direction (Isoda and Hikosaka, 2007).

Notably, in the current task, the same cue persisted across the prompt and execution blocks to induce a change in the context of the same sensory information—from being necessary to unnecessary to complete the task. Thus, the SMC may guide its modulatory activity based not only on the semantics of the task-relevant information but also on the context of the information. If the latter was the case, it is likely that the inhibitory modulation would no longer be observed when new task-relevant information arises, and additional motor planning is required (e.g., active navigation). Consistently, the frontoparietal neural activity in non-human-primates have been shown to sustain when additional information regarding the task becomes available during movements (Baldauf, et al., 2008; Siegel, et al., 2015) and a subset of pre-SMA neurons have been shown to respond selectively when new motor goals had to be encoded according to similar visual stimuli consisting of different patterns of the same elements (Tanji and Shima, 1994). Furthermore, SMC damage in humans has been implicated in positive motor dysfunctions, such as, the alien hand syndrome (Della Sala, Marchetti, & Spinnler, 1991; Feinberg, Schindler, Flanagan, & Haber, 1992) and nonintentional utilization behaviour (Boccardi, Della Sala, Motto, & Spinnler, 2002; Sumner, et al., 2007), showcasing the potential consequences of disturbances in context monitoring and the lack of task-irrelevant sensory information inhibition.

The observed pattern of diffuse BOLD activity is also consistent with our model which posits that further task-relevant information is extracted once it enters the frontoparietal regions from the higher order sensory cortices, and the recurrent information flow iteratively allows for integration and encoding of motor goals. Significant BOLD activations were observed in the SPL and IPS (in particular, the mIPS) in the PPC, and the PMC in the LPFC during the prompt blocks. The SPL, especially the left, is involved in processing of spatial configuration of one's own body parts (Felician, et al., 2004; Guariglia, Piccardi, Puglisi

Allegra, & Traballesi, 2002). The early SPL activation is thus likely to reflect the extraction of proprioceptive information necessary for the motor planning of isolated effector movements. The IPS is involved in motor planning (Connolly, Goodale, Menon, & Munoz, 2002; Connolly, et al., 2003), storing spatial working memory (Mackey, Devinsky, Doyle, Golfinos, & Curtis, 2016), and goal-encoding (Baldauf, et al., 2008; Medendorp, et al., 2006). The PMC has also been implicated in motor goal encoding (Binkofski, et al., 1999; Bremmer, et al., 2001) and goal encoding (Pesaran, Nelson, & Andersen, 2006), and multimodal information integration (Hoshi and Tanji, 2000). Furthermore, inferior PMC has been implicated in language processing (Binder, et al., 1997; Poldrack, et al., 1999) and the lateral PMC has been specifically implicated in integration of motor-target and body-part information in both humans (Medendorp, et al., 2005) and nonhuman primates (Hoshi and Tanji, 2000). Consistently, somatosensory/proprioceptive information from the SPL (Jones and Powell, 1970; Pandya and Kuypers, 1969) and visuospatial information from the IPS (Johnson, Ferraina, & Caminiti, 1993; Tanne, Boussaoud, Boyer-Zeller, & Rouiller, 1995) both converge in the PMd. As per our model posits and the current results suggest, previous studies have alluded that this frontoparietal interaction could be necessary for the accumulation of sensory information for a sufficient motor goal to be encoded, highlighting importance of graded functional specialization (Siegel, et al., 2012, 2015; Wang, 2008).

An interesting extension of the current work may be to investigate how the constituent movements of an encoded motor goal, namely the *motor programs* (Klapp, 1995; Wright, Black, Immink, Brueckner, & Magnuson, 2004), are represented within the framework of the proposed model. This study demonstrates how specific motor goals, as a whole, are encoded; but it does not show how the qualitative facets of the goals are distributed across the network. Combining the current protocol used, along with dissociative transient disruption methods (e.g., transcranial magnetic stimulation), may potentially provide some insights into the question raised above. For example, considering the current model and results, predictive activity rising either early in the frontoparietal regions or the immediately prior to the movement execution in the SMC may, in part, reflect the specific motor programs. Poizner et al. (2012) have shown that transient disruptions to the IPS or the arm region of the M1, but not SMC, during a pantomime task (mimicking the motion for slicing) resulted in accuracy and timing deficits in healthy individuals. Interestingly, only in instances of the IPS disruption, the participants reported that they were aware of the motor goal at hand. However, they could not control the effector to perform the movements as desired. Thus, it seems that when the IPS is disrupted, the abstract concept of the motor goal remains intact as whole, however, the underlying motor programs to explicitly perform the movement are affected, suggesting that the IPS may specifically contribute to the process of representing the motor programs (albeit not exhaustively).

4.1 | Caveats

Given the relatively small sample size of this study, a potential concern is the generalizability of the proposed model. However, all the results were significant and robustly support the proposed model, and as

described above, they were consistent with many previous human and animal studies that demonstrated the putative roles of the dorsal motor network regions during movement planning and execution. Furthermore, we took measures to reduce the likelihood of reducing false positive results, by using a more stringent p value threshold during individual-level fMRI analysis, extracting the BOLD signals in native space, correcting for multiple comparisons, and providing multiple measures of cortical information flow.

In particular, given that the major goal of this study was to investigate the temporal dynamics of cortical information flow, we controlled for the potential differences in HRFs across the dorsal motor network areas. Inter-regional differences in HRFs are critical when it comes to spatiotemporal dynamic analysis and Granger causality analysis. This is because both analyses are based on temporal precedence, and heterogeneous HRFs can essentially render the observed temporal differences irrelevant. In other words, neural activity occurring earlier in area A than area B can be observed first in BOLD activity of area B than A (Friston, 2009). Thus, heterogeneous HRFs are often used as the crux of the argument against using Granger causality analysis on fMRI data, with the seminal study by David et al. (2008) being presented as empirical evidence.

Indeed, the study by David et al. shows how heterogeneous HRFs can affect the results of causality analyses, using a multimodal approach in a well-established absence epilepsy mouse model that is presented in the form of spontaneous spike-and-wave discharges originating from the somatosensory cortex. However, the authors also demonstrate that the issue of heterogeneous HRFs can be controlled for through the removal of the hemodynamic effects from the BOLD signals using deconvolution methods. The authors performed simultaneous cranial electrocorticography (EEG) and fMRI, and intracranial electrocorticography (iEEG) in regions of strong BOLD activation during absence epilepsy. Using the simultaneous EEG-fMRI recordings, regional-specific HRFs were estimated then used to deconvolute the BOLD signal for removal of hemodynamic effects. The results revealed heterogeneous HRFs in each region of strong BOLD activation during the epilepsy—the somatosensory cortex, the thalamus, and the striatum. Consistently, the origins of absence epilepsy (i.e., the somatosensory cortex) could be correctly estimated from the BOLD signal timeseries extracted from these areas using Granger-causality analysis, only when the signals were deconvoluted with the estimated region-specific HRFs. The authors validate the results by demonstrating that the origin of the absence epilepsy was identified as the somatosensory cortex by performing Granger causality analysis with the iEEG signals from the same regions.

However, simultaneous EEG-fMRI recordings require expensive, specialized equipment, and remain unavailable in most sites. Thus, in this body of work, we performed hemodynamic deconvolution on the BOLD signal as per David et al., however, using a blind approach (Wu, et al., 2013) to control for the confound of heterogeneous HRFs driving the observed spatiotemporal dynamics and the direction of G-causal relationships (Section 2). This model requires forming a hypothetical model of neural states to solve for the HRF term in the hemodynamic convolution equation. All points of positive BOLD signal deviation above an arbitrary threshold (1 SD) from the mean are treated as an event of neural activity, which could capture the hidden neural states during the task, as well as rest. A simple double-gamma function is used to convolute the hypothetical neural states to form the model. Importantly, the HRF delay term is optimized for each voxel, thus, a wide range of potential variance in HRFs is captured across the brain. This allows for estimation of voxel-specific HRF, and approximation of the neural states underlying the observed BOLD signal through deconvolution as per David et al.'s study. In addition, subjecting the nondeconvoluted BOLD signals to exactly the same activation onset and offset latency (Supporting Information, Figure 4), cross-correlation analysis (Supporting Information, Figure 5), and decoding performance (Supporting Information, Figure 3) analysis revealed consistent results, suggesting that the observed effects were not driven by the region-specific HRF differences or the deconvolution process, but indeed by the different stages of motor goal planning and execution.

5 | CONCLUSION

This study shows for the first time, how the human dorsal motor network coherently plans and executes selective movement goals, in turn, providing compelling evidence for our proposed model of movement planning and execution. Our model proposes that early extraction of task-relevant information in the higher order sensory cortices allows for goal-dependent variances in input levels between the on and off subregions of the dorsal motor network. Then, through spatially dynamic goal-dependent subregional patterns of positive and negative feedback loops between the SMC and the frontoparietal areas, the SMC can monitor the accumulating information downstream and facilitate the activity in the on subregion while inhibiting that in the off subregion according to the goal. This iterative process allows the areas of the dorsal-motor network to collectively encode selective goals and perform movement monitoring and control. Consequently, we conclude that the selective motor goal encoding and execution rely on goal-dependent differences in subregional recurrent information flow patterns across the long-range dorsal motor network areas that exhibit graded functional specialization.

ORCID

Peter E. Yoo http://orcid.org/0000-0002-0014-5539

REFERENCES

Archambault, P. S., Caminiti, R., & Battaglia-Mayer, A. (2009). Cortical mechanisms for online control of hand movement trajectory: The role of the posterior parietal cortex. *Cerebral Cortex*, *19*(12), 2848–2864.

Avants, B., Tustison, N., & Song, G. (2011). Advanced normalization tools (ANTS). *Release*, *1*, 5.

Baldauf, D., Cui, H., & Andersen, R. A. (2008). The posterior parietal cortex encodes in parallel both goals for double-reach sequences. *Journal of Neuroscience*, *28*(40), 10081–10089.

Barnett, L., & Seth, A. K. (2014). The MVGC multivariate Granger causality toolbox: A new approach to Granger-causal inference. *Journal of Neuroscience Methods*, *223*, 50–68.

Batista, A. P., & Andersen, R. A. (2001). The parietal reach region codes the next planned movement in a sequential reach task. *Journal of Neurophysiology*, *85*(2), 539–544.

Binder, J. R., Frost, J. A., Hammeke, T. A., Cox, R. W., Rao, S. M., & Prieto, T. (1997). Human brain language areas identified by functional magnetic resonance imaging. *Journal of Neuroscience*, *17*, 353–362.

Binkofski, F., Buccino, G., Stephan, K. M., Rizzolatti, G., Seitz, R. J., & Freund, H. J. (1999). A parieto-premotor network for object manipulation: Evidence from neuroimaging. *Experimental Brain Research*, *128*(1–2), 210–213.

Boccardi, E., Della Sala, S., Motto, C., & Spinnler, H. (2002). Utilisation behaviour consequent to bilateral SMA softening. *Cortex*, *38*(3), 289–308.

Bremmer, F., Schlack, A., Shah, N. J., Zafiris, O., Kubischik, M., Hoffmann, K., . . . Fink, G. R. (2001). Polymodal motion processing in posterior parietal and premotor cortex: A human fMRI study strongly implies equivalencies between humans and monkeys. *Neuron*, *29*(1), 287–296.

Connolly, J. D., Andersen, R. A., & Goodale, M. A. (2003). FMRI evidence for a 'parietal reach region' in the human brain. *Experimental Brain Research*, *153*(2), 140–145.

Connolly, J. D., Goodale, M. A., Menon, R. S., & Munoz, D. P. (2002). Human fMRI evidence for the neural correlates of preparatory set. *Nature Neuroscience*, *5*(12), 1345–1352.

Cunnington, R., Windischberger, C., Deecke, L., & Moser, E. (2002). The preparation and execution of self-initiated and externally-triggered movement: A study of event-related fMRI. *NeuroImage*, *15*(2), 373–385.

Cunnington, R., Windischberger, C., Robinson, S., & Moser, E. (2006). The selection of intended actions and the observation of others' actions: A time-resolved fMRI study. *NeuroImage*, *29*(4), 1294–1302.

David, O., Guillemain, I., Saillet, S., Reyt, S., Deransart, C., Segebarth, C., & Depaulis, A. (2008). Identifying neural drivers with functional MRI: An electrophysiological validation. *PLoS Biology*, *6*(12), e315–e397.

Della Sala, S., Francescani, A., & Spinnler, H. (2002). Gait apraxia after bilateral supplementary motor area lesion. *Journal of Neurology, Neurosurgery & Psychiatry*, *72*(1), 77–85.

Della Sala, S., Marchetti, C., & Spinnler, H. (1991). Right-sided anarchic (alien) hand: A longitudinal study. *Neuropsychologia*, *29*(11), 1113–1127.

Desikan, R. S., Segonne, F., Fischl, B., Quinn, B. T., Dickerson, B. C., Blacker, D., . . . Killiany, R. J. (2006). An automated labeling system for subdividing the human cerebral cortex on MRI scans into gyral based regions of interest. *NeuroImage*, *31*(3), 968–980.

Feinberg, T. E., Schindler, R. J., Flanagan, N. G., & Haber, L. D. (1992). Two alien hand syndromes. *Neurology*, *42*(1), 19–24.

Felician, O., Romaiguere, P., Anton, J. L., Nazarian, B., Roth, M., Poncet, M., & Roll, J. P. (2004). The role of human left superior parietal lobule in body part localization. *Annals of Neurology*, *55*(5), 749–751.

Friston, K. (2009). Causal modelling and brain connectivity in functional magnetic resonance imaging. *PLoS Biology*, *7*(2), e33.

Gaveau, V., Pisella, L., Priot, A. E., Fukui, T., Rossetti, Y., Pelisson, D., & Prablanc, C. (2014). Automatic online control of motor adjustments in reaching and grasping. *Neuropsychologia*, *55*, 25–40.

Geißler, A., Fischmeister, F. P. S., Grabner, G., Wurnig, M., Rath, J., Foki, T., . . . Robinson, S. D. (2013). Comparing the microvascular specificity of the 3- and 7-T BOLD response using ICA and susceptibility-weighted imaging. *Frontiers in Human Neuroscience*, *7*, 474.

Glover, S., Miall, R. C., & Rushworth, M. F. (2005). Parietal rTMS disrupts the initiation but not the execution of on-line adjustments to a perturbation of object size. *Journal of Cognitive Neuroscience*, *17*(1), 124–136.

Guariglia, C., Piccardi, L., Puglisi Allegra, M. C., & Traballesi, M. (2002). Is autotopoagnosia real? EC says yes. A case study. *Neuropsychologia*, *40*(10), 1744–1749.

Hoshi, E., & Tanji, J. (2000). Integration of target and body-part information in the premotor cortex when planning action. *Nature*, *408*(6811), 466–470.

Isoda, M., & Hikosaka, O. (2007). Switching from automatic to controlled action by monkey medial frontal cortex. *Nature Neuroscience*, *10*(2), 240–248.

Jenkinson, M., Beckmann, C. F., Behrens, T. E., Woolrich, M. W., & Smith, S. M. (2012). FSL. *NeuroImage*, *62*(2), 782–790.

Johnson, P. B., Ferraina, S., & Caminiti, R. (1993). Cortical networks for visual reaching. *Experimental Brain Research*, *97*(2), 361–365.

Jones, E. G., & Powell, T. P. (1970). An anatomical study of converging sensory pathways within the cerebral cortex of the monkey. *Brain: A Journal of Neurology*, *93*(4), 793–820.

Kennerley, A. J., Mayhew, J. E., Redgrave, P., & Berwick, J. (2010). Vascular origins of BOLD and CBV fMRI signals: Statistical mapping and histological sections compared. *The Open Neuroimaging Journal*, *4*, 1–8.

Klapp, S. T. (1995). Motor response programming during simple and choice reaction time: The role of practice. *Journal of Experimental Psychology: Human Perception and Performance*, *21*(5), 1015–1027.

Krainik, A., Lehericy, S., Duffau, H., Vlaicu, M., Poupon, F., Capelle, L., . . . Marsault, C. (2001). Role of the supplementary motor area in motor deficit following medial frontal lobe surgery. *Neurology*, *57*(5), 871–878.

Mackey, W. E., Devinsky, O., Doyle, W. K., Golfinos, J. G., & Curtis, C. E. (2016). Human parietal cortex lesions impact the precision of spatial working memory. *Journal of Neurophysiology*, *116*(3), 1049–1054.

Marques, J. P., Kober, T., Krueger, G., van der Zwaag, W., Van de Moortele, P. F., & Gruetter, R. (2010). MP2RAGE, a self bias-field corrected sequence for improved segmentation and T1-mapping at high field. *NeuroImage*, *49*(2), 1271–1281.

Medendorp, W. P., Goltz, H. C., Crawford, J. D., & Vilis, T. (2005). Integration of target and effector information in human posterior parietal cortex for the planning of action. *Journal of Neurophysiology*, *93*(2), 954–962.

Medendorp, W. P., Goltz, H. C., & Vilis, T. (2006). Directional selectivity of BOLD activity in human posterior parietal cortex for memory-guided double-step saccades. *Journal of Neurophysiology*, *95*(3), 1645–1655.

Nachev, P., Kennard, C., & Husain, M. (2008). Functional role of the supplementary and pre-supplementary motor areas. *Nature Reviews. Neuroscience*, *9*(11), 856–869.

Nachev, P., Rees, G., Parton, A., Kennard, C., & Husain, M. (2005). Volition and conflict in human medial frontal cortex. *Current Biology, 15*(2), 122–128.

Pandya, D. N., & Kuypers, H. G. (1969). Cortico-cortical connections in the rhesus monkey. *Brain Research, 13*(1), 13–36.

Pesaran, B., Nelson, M. J., & Andersen, R. A. (2006). Dorsal premotor neurons encode the relative position of the hand, eye, and goal during reach planning. *Neuron, 51*(1), 125–134.

Picard, N., & Strick, P. L. (1996). Motor areas of the medial wall: A review of their location and functional activation. *Cerebral Cortex, 6*(3), 342–353.

Picard, N., & Strick, P. L. (2001). Imaging the premotor areas. *Current Opinion in Neurobiology, 11*(6), 663–672.

Poizner, H., Lancaster, J., Tunik, E., Narayana, S., Franklin, C., Rogers, W., ... Robin, D. A. (2012). Towards a healthy human model of neural disorders of movement. *IEEE Transactions on Neural Systems and Rehabilitation Engineering, 20*(6), 853–857.

Poldrack, R. A., Wagner, A. D., Prull, M. W., Desmond, J. E., Glover, G. H., & Gabrieli, J. D. (1999). Functional specialization for semantic and phonological processing in the left inferior prefrontal cortex. *NeuroImage, 10*(1), 15–35.

Ridderinkhof, K. R., Ullsperger, M., Crone, E. A., & Nieuwenhuis, S. (2004). The role of the medial frontal cortex in cognitive control. *Science (New York, N.Y.), 306*(5695), 443–447.

Santucci, D. M., Kralik, J. D., Lebedev, M. A., & Nicolelis, M. A. (2005). Frontal and parietal cortical ensembles predict single-trial muscle activity during reaching movements in primates. *European Journal of Neuroscience, 22*(6), 1529–1540.

Scherberger, H., Jarvis, M. R., & Andersen, R. A. (2005). Cortical local field potential encodes movement intentions in the posterior parietal cortex. *Neuron, 46*(2), 347–354.

Siegel, M., Buschman, T. J., & Miller, E. K. (2015). Cortical information flow during flexible sensorimotor decisions. *Science, 348*(6241), 1352–1355.

Siegel, M., Donner, T. H., & Engel, A. K. (2012). Spectral fingerprints of large-scale neuronal interactions. *Nature Reviews. Neuroscience, 13*, 121–134.

Singer, W. (2013). Cortical dynamics revisited. *Trends in Cognitive Sciences, 17*(12), 616–626.

Sumner, P., Nachev, P., Morris, P., Peters, A. M., Jackson, S. R., Kennard, C., & Husain, M. (2007). Human medial frontal cortex mediates unconscious inhibition of voluntary action. *Neuron, 54*(5), 697–711.

Tanji, J., & Shima, K. (1994). Role for supplementary motor area cells in planning several movements ahead. *Nature, 371*(6496), 413–416.

Tanne, J., Boussaoud, D., Boyer-Zeller, N., & Rouiller, E. M. (1995). Direct visual pathways for reaching movements in the macaque monkey. *NeuroReport, 7*(1), 267–272.

Triantafyllou, C., Hoge, R. D., Krueger, G., Wiggins, C. J., Potthast, A., Wiggins, G. C., & Wald, L. L. (2005). Comparison of physiological noise at 1.5 T, 3 T and 7 T and optimization of fMRI acquisition parameters. *NeuroImage, 26*(1), 243–250.

Ullsperger, M., & von Cramon, D. Y. (2001). Subprocesses of performance monitoring: A dissociation of error processing and response competition revealed by event-related fMRI and ERPs. *NeuroImage, 14*(6), 1387–1401.

van der Zwaag, W., Francis, S., Head, K., Peters, A., Gowland, P., Morris, P., & Bowtell, R. (2009). fMRI at 1.5, 3 and 7 T: Characterising BOLD signal changes. *NeuroImage, 47*(4), 1425–1434.

Wang, X. J. (2008). Decision making in recurrent neuronal circuits. *Neuron, 60*(2), 215–234.

Wong, Y. T., Fabiszak, M. M., Novikov, Y., Daw, N. D., & Pesaran, B. (2016). Coherent neuronal ensembles are rapidly recruited when making a look-reach decision. *Nature Neuroscience, 19*(2), 327–334.

Wright, D. L., Black, C. B., Immink, M. A., Brueckner, S., & Magnuson, C. (2004). Long-term motor programming improvements occur via concatenation of movement sequences during random but not during blocked practice. *Journal of Motor Behavior, 36*(1), 39–50.

Wu, G. R., Liao, W., Stramaglia, S., Ding, J. R., Chen, H., & Marinazzo, D. (2013). A blind deconvolution approach to recover effective connectivity brain networks from resting state fMRI data. *Medical Image Analysis, 17*(3), 365–374.

Yoo, P. E., John, S. E., Farquharson, S., Cleary, J. O., Wong, Y. T., Ng, A., ... Moffat, B. A. (2017). 7T-fMRI: Faster temporal resolution yields optimal BOLD sensitivity for functional network imaging specifically at high spatial resolution. *NeuroImage.*

SUPPORTING INFORMATION

Additional Supporting Information may be found online in the supporting information tab for this article.